# Fermi-Surface Studies in SnTe†*

H. T. Savage
*Naval Ordnance Laboratory, Silver Spring, Maryland* 20910
*and University of Maryland, College Park, Maryland* 20742

and

Bland Houston and J. R. Burke, Jr.
*Naval Ordnance Laboratory, Silver Spring, Maryland* 20910
(Received 32 February 1972)

We have used the de Haas–van Alphen effect and Shubnikov–de Haas effect at temperatures from 1.6 to 7.9 K to investigate the Fermi surface of SnTe. Nine samples were studied covering a range in carrier concentration from $5\times10^{19}$ to $5\times10^{20}$ cm$^{-3}$. The nature of the data is such that they divide into two regions in carrier concentration, a normal one at or above $3.6\times10^{20}$ cm$^{-3}$ and an anomalous one at or below $2.1\times10^{20}$ cm$^{-3}$. In the normal region one extremal cross section was observed at each orientation describing a pocket elongated in a ⟨111⟩ direction and located at the $L$ point. In addition, oscillations describing a second set of pockets elongated in a ⟨100⟩ direction were observed. At a carrier concentration of $3.6\times10^{20}$ cm$^{-3}$, Dingle temperatures and cyclotron masses of 21.6 K and $0.125m_0$ and 17.3 K and $0.094m_0$ were measured for the ⟨111⟩ and ⟨100⟩ pockets, respectively. At about this carrier concentration a density of states of $6\times10^{21}$ (eV cm$^3$)$^{-1}$ was computed from the data and is in fair agreement with the density of states computed from heat-capacity measurements. In the anomalous region a number of extremal cross sections describing one pocket at the $L$ point were observed at each orientation. The shapes of the constant-energy surfaces described by the data are in poor agreement with the results of existing band calculations.

## I. INTRODUCTION

### A. Stoichiometry and Carrier Generation

SnTe is a IV-VI compound that has the NaCl structure. In perfectly stoichiometric and chemically pure form it would be an intrinsic semiconductor. Its valence-conduction band gap is believed to be direct, or nearly so. However, it is evident in the phase diagram[1] shown in Fig. 1 that at finite temperatures the equilibrium state has a Sn deficiency. As a result the material is extrinsic with a carrier concentration of two holes per Sn vacancy (the 2 will be justified later). If SnTe is maintained at its Sn-rich solubility limit, higher temperatures give higher equilibrium carrier concentrations. The chemical diffusion constant of Sn in SnTe is so small below 600 K that in bulk samples equilibrium vacancy concentrations corresponding to higher temperatures are "frozen in."

A plausible explanation for SnTe having the electrical properties of a "dilute metal" (except having holes instead of electrons for carriers) is provided by the results of a rather complicated band calculation for PbTe, a similar IV-VI compound, of Parada and Pratt.[2] They find that the perturbation introduced by removing one Pb atom moves two energy levels in a Pb $s$-like valence band well above the bottom of the conduction band. Since the removal of one neutral Pb atom removes four valence electrons, two holes are created at the top of the uppermost valence band. This possibly explains why carrier freeze-out is not observed in PbTe (or SnTe). No evidence of impurity banding (the vacancies are the impurities) in the band gap has been found in PbTe or SnTe.

### B. Carrier Counting

Houston *et al.*[3] have attempted to relate the carrier concentration $p$ to a nominal carrier concentration $p^*$ by a constant $r$, where

$$p^* \equiv 1/Re \tag{1}$$

and

$$p = rp^* . \tag{2}$$

$R$ is the weak-field Hall coefficient measured at or below 77 K and $e$ is the electronic charge. They measured the change in $p^*$ due to the diffusion of known amounts of Cu and Sn into $Sn_{1-x}Te$ samples. Their study implied a value of 0.6 for $r$. Their study covered a range of $p^*$ from $2\times10^{20}$ to $2\times10^{21}$ cm$^{-3}$. This work has been substantiated by that of Brebrick.[4]

### C. Band Calculations

Tung and Cohen[5] have used the empirical pseudopotential method to calculate the band structure of SnTe. They find the absolute valence-band maximum in the zone face slightly away from the $L$ point. The $\vec{k}\cdot\vec{p}$ calculation about $L$ of Rabii[6] is in

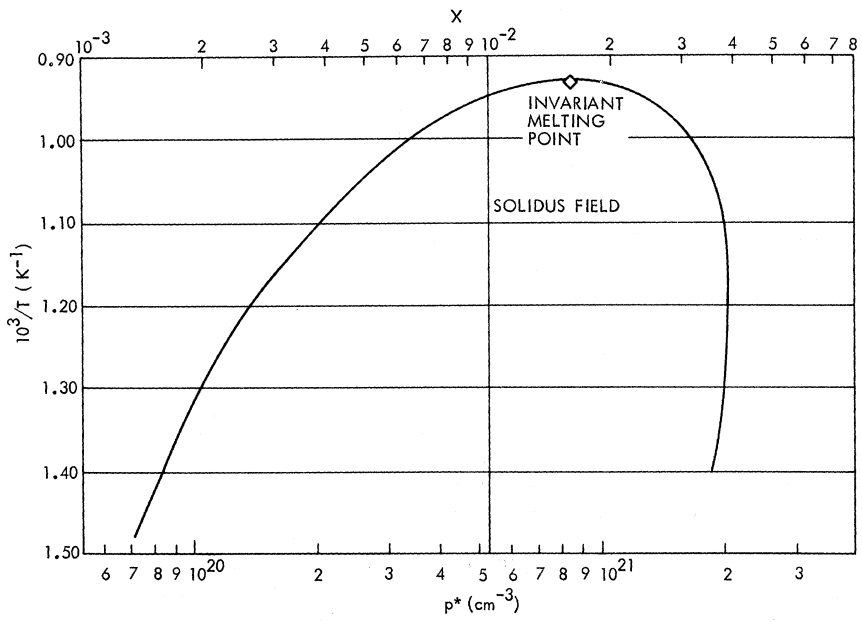


FIG. 1. Phase diagram of $Sn_{1-x}Te$. Left boundary of the solidus field is the solubility limit of Sn.

agreement with this. Both find a saddle point at $L$. Another $\vec{k}\cdot\vec{p}$ calculation at $L$ by Tsu *et al.*[7] leads to a "dumbbell" shape. Their matrix elements are determined from experimental data. Dimmock[8] has developed a dispersion relation for SnTe. The valence-band maximum is away from $L$ in a ⟨111⟩ direction. As the carrier concentration is increased the Fermi surface (FS) evolves from two bubbles to a dumbbell to a convex surface. All of the above surfaces have the axis of revolution along ⟨111⟩. Tsang and Cohen[9] have done a pseudopotential calculation in great detail around $L$. The resulting constant-energy surface has threefold symmetry around ⟨111⟩ (see Ref. 9 for detailed drawings). Herman *et al.*[10] find the valence-band maxima at $L$ using an orthogonalized-plane-wave (OPW) technique. Bernick and Kleinman[11] using a pseudopotential technique find the valence maximum at $L$. Three of the calculations[5,6,11] find secondary maxima on the $\Sigma$ axis and tertiary maxima on the $\Delta$ axis. All of these maxima are in the same band as the $L$ maxima.

### D. Purpose and Technique

In spite of the considerable attention given to SnTe during the past 10 years, many of its physical properties are the subject of controversy.[12,13] Though the qualitative features of its band structure are probably fairly clearly established, the details which are most important in determining its electrical transport properties have not been determined. One of the most powerful experimental methods for obtaining this type of detailed band-structure information is the determination of the FS by means of measurements of the Shubnikov–de Haas (SdH) and de Haas–van Alphen (dHvA) effects. In spite of the high vacancy concentrations, these methods prove to be very useful in SnTe.

The oscillation of the diamagnetism as a function of magnetic field is called the dHvA effect. Its origin is the same as that of SdH effect,[14] i.e., a small oscillatory component of the density of states at the FS. The period of the oscillation is inversely proportional to the area of an extremal cross section of the FS normal to the magnetic field.

Initially, work consisted entirely of SdH measurements.[15,16] When the SdH data proved to be quite complex we shifted to a measurement of the dHvA effect because the theory of the dHvA effect is simpler and more general. However, except for qualifications to be delineated later, the results of the two experiments are the same.

Brailsford[17] has derived an expression for the oscillatory part of the free energy of free carriers with an arbitrary dispersion relation. The method is similar to the derivation of Lifshitz and Kosevich[18] except that the influence of impurity scattering is included. In different notation the result of the Brailsford derivation is

$$M=\left(\frac{eH}{2\pi\hbar c}\right)^{1/2}\left(\left|\frac{\partial^2 A(k_z)}{\partial k_z^2}\right|_{k_z=k_{z0}}\right)^{-1/2}\left(\cos\theta+\sin\theta\,\frac{1}{A}\frac{\partial A}{\partial\theta}\right)\left(\frac{kTA}{\pi H}\right)\sum_{l=1}^{\infty}\frac{\sin[2\pi l(\hbar cA/2\pi eH-\gamma)\mp\frac{1}{4}\pi]e^{-\pi l/\omega_c\tau}}{l^{1/2}\sinh(2\pi^2 lkTmc/\hbar eH)}\cos\left(\frac{\pi lgm}{2m_0}\right), \tag{3}$$

where (in cgs units) $M$ is the oscillatory component of the magnetization at angle $\theta$ to the applied field $H$; $T$ is the temperature; $A$ is the extremal cross-sectional area of the FS; $k_z$ is the component of a vector in reciprocal space in the direction of the magnetic field; $k_{z0}$ is the location in reciprocal space of the extremal area normal to the field; $\gamma$ is a phase factor ($\frac{1}{2}$ for free electrons); $\tau$ is the lifetime for impurity scattering for the extremal area of interest; $m$ is the cyclotron mass; $\omega_c$ is the cyclotron frequency; and $m_0$ is the free-electron mass.

The use of this definition of $\tau$ is valid as long as the scattering is unaffected by the presence of a magnetic field. It is conventional to define a pseudotemperature called the Dingle temperature to express the lifetime for impurity scattering as follows:

$$T_D \equiv (\hbar/2\pi k)\tau^{-1} . \tag{4}$$

The spin factor $\cos(\pi lgm/2m_0)$ has been added from Ref. 18; $g$ is the effective gyromagnetic ratio.

A frequency $F$ can be defined as

$$F \equiv (\hbar c/2\pi e)A . \tag{5}$$

The oscillation of a component of the resistivity at low temperature is called the SdH effect.[14] The oscillatory terms in the SdH effect have the same form as Eq. (3) with slightly different amplitude factors. These differences are not important for our analysis.

The dHvA measurements were done by the field-modulation technique using an apparatus similar to that of Goldstein *et al.*[19] The modulation field was in the direction of the dc field and the signal detected at twice the fundamental frequency. The sample rotator was a modification of the one developed by Thorsen and Berlincourt.[20] Details of the construction of the apparatus are available in Ref. 21. The dHvA measurements were carried out in two superconducting magnets. One had a peak field of 50 kG and the other, 110 kG. The SdH work was done with a dc resistivity technique in the 150-kG high-field facility at the Naval Research Laboratory.

Analysis of the data via Eq. (3) can determine the shape of the FS from the frequencies. In addition, the cyclotron mass $m$ can be determined from the temperature dependence of the amplitude, and the Dingle temperature $T_D$, from the field dependence of the amplitude. Such determinations will be described in Sec. III.

## II. MATERIAL PREPARATION

The samples were prepared using the following procedure. Large single crystals of $Sn_{1-x}Te$ were pulled from the melt by the Czochralski technique. These crystals were grown at the invariant melting composition ($x = 0.016$). Lower carrier concentrations were achieved by diffusing Sn into the samples. For reasonable diffusion times the samples must be small $0.03 \times 0.04 \times 0.03$ in.[3] being standard.

Two methods were used for controlling the amount of Sn diffused into the samples. In both methods Sn is electroplated onto the sample and diffused into it during a high-temperature anneal. In the first method, the amount of Sn plated onto the sample is controlled so that diffusing all of it into the sample will achieve the desired change in $x$. The anneal is then carried out at a temperature at which the final composition lies within the solidus field (Fig. 1). In the second method more Sn is plated onto the sample than is required to achieve the desired change in $x$. The temperature of the anneal is then controlled so that the desired value of $x$ lies at the solubility limit for Sn in SnTe. This temperature can be determined from the phase diagram. The anneal time at each temperature was determined during the phase-diagram studies by measurements of the Hall coefficients of samples obtained from a series of isothermal anneals. In order to reduce the required anneal times, the crystals were frequently subjected to a sequence of anneals at successively lower temperatures. In this sequence of anneals, most of the Sn is diffused into the sample at high temperatures where the diffusion is faster. The remainder is diffused in at lower temperatures where Sn is more soluble.

Properties characterizing the samples used in this experiment are shown in Table I. The quantities listed in the table are defined as follows: the Hall mobility

$$\mu_{77}^{*} \equiv R_{77}\sigma_{77} \tag{6}$$

and the conductivity mobility

$$\mu_{4.2} \equiv \sigma_{4.2}/pe . \tag{7}$$

Here $R$ is the weak-field Hall coefficient, $\sigma$ is the conductivity, and $p$ is the carrier concentration [Eq. (2)]. The subscripts denote the absolute temperature at which the quantity was determined. $R$ is independent of temperature below 100 K.

## III. EXPERIMENTAL RESULTS

### A. Data Reduction

Equation (3) contains parameters directly characterizing the FS. Extracting their values from the data is not straightforward in multiperiod data. The giant modulation technique[19] that is very useful in metals for frequency (extremal cross-sectional area) discrimination is difficult here because of the small FS (low frequencies) and poor $\omega_c\tau$ condi-

TABLE I. Sample characterization.

| Sample | $10^{-19}p^*$ ($cm^{-3}$) | $\mu_{77}^*$ ($cm^2\ V^{-1}\ sec^{-1}$) | $\mu_{4.2}$[a] ($cm^2\ V^{-1}\ sec^{-1}$) |
|---|---|---|---|
| 1001A | 7.2 | 3150 | |
| 1000 | 8.2 | 2700 | 14 000 |
| 676 | 10.6 | 2000 | 10 000 |
| 670 | 13.0 | 1600 | 7 200 |
| 647 | 35 | 420 | 1 300 |
| 652A[b] | 61 | 240 | 700 |
| 652B[b] | 61 | 240 | 700 |
| 1002[c] (as-grown) | 80 | 190 | 480 |

[a]Helium-temperature conductivity mobility is from Fig. 2. The carrier concentration is assumed to be $0.6p^*$. The 0.6 factor is from chemical composition studies (Ref. 3).

[b]652A, 652B, and the sample on which the Hall measurement was performed were cut from the same crystal and prepared together.

[c]Values listed for sample 1002 are typical values from measurements on other samples from the same crystal.

tions. The modulation fields required would be the order of 1 kG at a dc field of 20 kG. The use of a dc field sweep proportional to inverse time with electronic filtering is also difficult because the resulting real-time frequencies would be extremely low. For these reasons the Fourier-analysis technique given in Ref. 21 was used to sort out the various frequencies present.

Data used for the cyclotron mass and Dingle temperature determinations contained only one frequency so that conventional analysis techniques could be used. The following expression was used in a least-squares fit to the data to determine the cyclotron masses:

$$\ln\left(\frac{A_1}{A_2}\right)=\ln\left(\frac{T_1}{T_2}\,\frac{\sinh(2\pi^2kT_2/\beta H)}{\sinh(2\pi^2kT_1/\beta H)}\right), \tag{8}$$

where $A$ is the amplitude at temperature $T$ and field $H$, and $\beta=eh/mc$.

The Dingle temperature $T_D$ was determined from a least-squares fit to the following relation:

$$\ln\left(\frac{A_1}{A_2}\right)=\ln\left\{\left(\frac{H_2}{H_1}\right)^{9/2}\left(\frac{\sinh(2\pi^2kT/\beta H_2)}{\sinh(2\pi^2kT/\beta H_1)}\right)\times\exp\left[-\frac{2\pi^2kT_D}{\beta}\left(\frac{1}{H_1}-\frac{1}{H_2}\right)\right]\right\}. \tag{9}$$

This expression is valid in the weak-field modulation limit.[19] Fits to data taken below 2 K (where the data are approximately temperature independent) gave essentially the same values for the Dingle temperatures as the data taken at higher temperatures. This temperature independence serves as a check on the over-all analysis.

### B. Representation of Data in Terms of Shape of FS

#### *1. Dispersion Relation*

When the field is turned more than $\pm 60°$ from the direction in which the minimum frequency is observed the oscillations lose amplitude and become unobservable because of an increase in cyclotron mass and possibly increased scattering. The data over this range suggest a FS consisting of approximately cylindrically shaped pockets positioned at noncentral high-symmetry points of the Brillouin zone. It is therefore convenient to consider the following dispersion relation:

$$D=k_x^2+k_y^2+Ck_z^2\,. \tag{10}$$

Let the field point in $k_z$ direction. In order to express the frequencies of the above surface as a function of sample orientation with respect to the field, it is convenient to consider the effects of two rotations. The two rotations are defined by the angles $\theta'$ and $\gamma$. The angle $\gamma$ is the complement of the angle between the sample rotator axis and the axis of rotational symmetry of the pocket. $\theta'$ is an angle of rotation about the sample rotator axis. $\theta'$ plus a constant $\theta_0$ corresponds to the sample rotator angle $\theta$. With the appropriate substitutions in Eq. (10) one obtains the equation for the extremal cross-sectional area $A$:

$$A=\frac{\pi D}{\cos\theta'(\cos^2\gamma+C\sin^2\gamma)^{1/2}}\times\left(1+\frac{C}{\cos^2\gamma+C\sin^2\gamma}\tan^2\theta'\right)^{-1/2}$$
$$=(\pi D/c)\left[1+(1/C-1)\cos^2\theta'\sin^2\gamma\right]^{-1/2}\,.$$

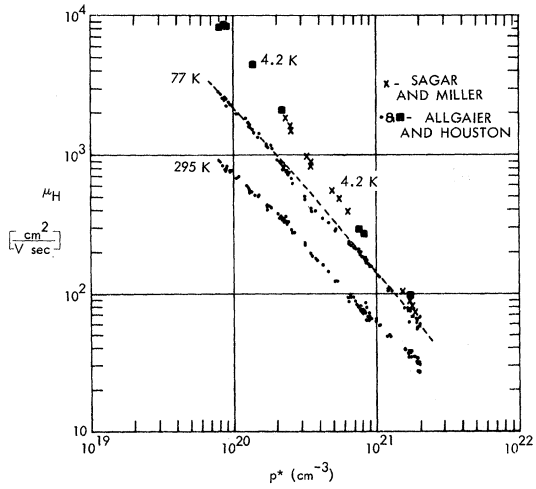


FIG. 2. Hall mobility of SnTe as a function of $p^*(1/Re)$, where $R$, the low-field Hall coefficient, is measured at 77 K) (Ref. 22).

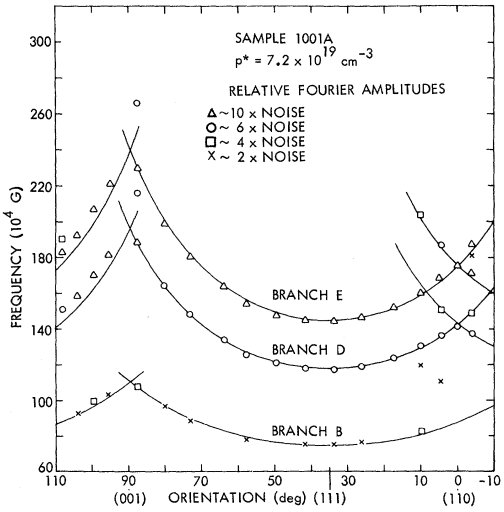


FIG. 3. dHvA frequencies vs orientation. Solid curves represent a calculation based upon the dispersion relation given by Eq. (10).

Since the frequency $F$ is $\hbar c/2\pi e$ times the area in $k$ space, we have

$$F = [C_1/\cos(\theta - \theta_0)][1 + C_2 \tan^2(\theta - \theta_0)]^{-1/2}, \quad (11)$$

where

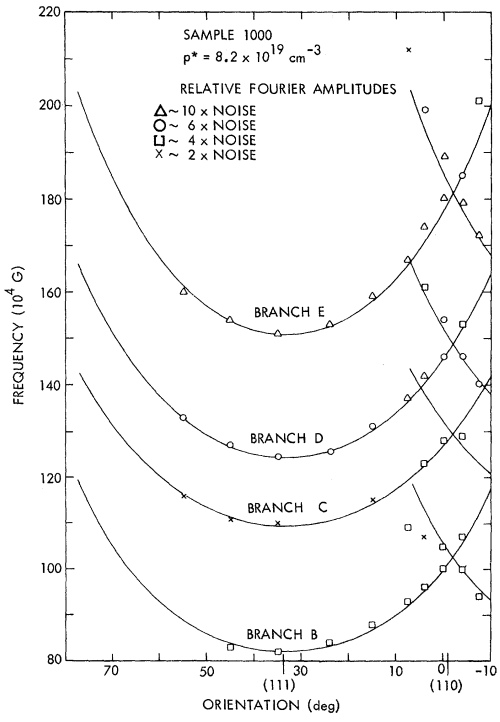


FIG. 4. dHvA frequencies vs orientation. Solid curves represent a calculation based upon the dispersion relation given by Eq. (10).

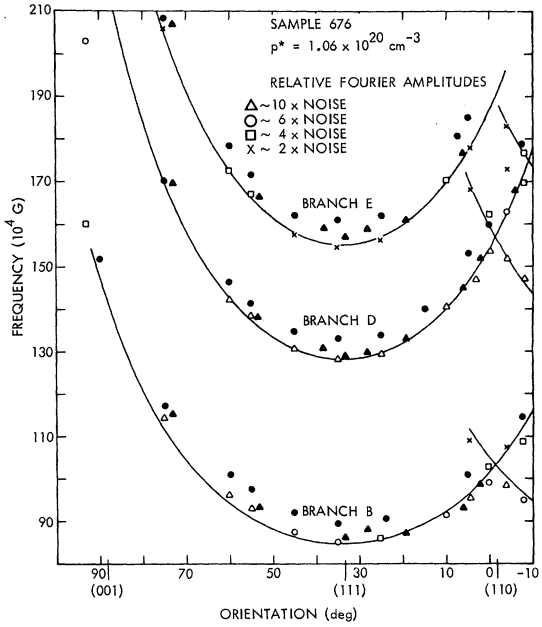


FIG. 5. Frequencies vs orientation. Solid curves represent a calculation based upon the dispersion relation given by Eq. (10). Circles are the SdH data. Triangles are dHvA data taken at higher fields (Table II).

$$C_1 = (\hbar D c/2e)(\cos^2\gamma + C \sin^2\gamma)^{-1/2} \quad (12)$$

and

$$C_2 = C(\cos^2\gamma + C \sin^2\gamma)^{-1}. \quad (13)$$

If only $\theta$ is varied, as is the case when the sample rotator is turned, the area minimizes at $\theta = \theta_0$.

### 2. *Data and Their Dispersion-Relation Representation*

The frequencies are plotted vs orientation in Figs. 3–10 for seven carrier concentrations. In these figures the points, unless otherwise noted, are the dHvA data. The curves are from a least-squares fit to Eq. (11). The relative Fourier amplitudes which are indicated in the figures are taken directly from transforms without any corrections for field range, field-modulation amplitude, and temperature. Frequency data are accurate to ±2%.

With $p^* \leq 3.5\times10^{20}$ cm$^{-3}$, the data at a specific orientation had from 3 to 5 frequencies describing one pocket at the $L$ point of the Brillouin zone. Each continuous curve of frequency vs orientation will be called a branch. The five branches with $p^* \leq 3.5\times10^{20}$ cm$^{-3}$ will be called $A$, $B$, $C$, $D$, and $E$.

The data of the first five samples have the parameters of Eq. (11) listed in Table II (including low- and high-field runs on sample 676). Since the axis of rotation is $[1\bar{1}0]$, $C_1$ of Eq. (11) repre-

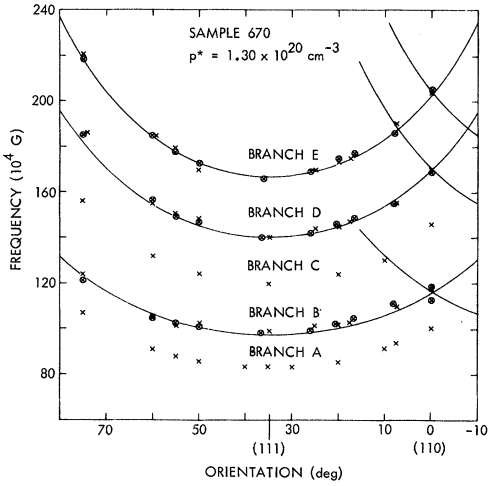


FIG. 6. Frequencies vs orientation. Solid curves represent a calculation based upon the dispersion relation given by Eq. (10). The circled points are the dHvA data. The uncircled points are the SdH data.

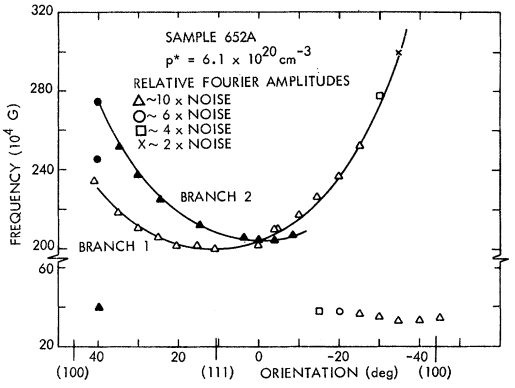


FIG. 8. dHvA frequencies vs orientation. Solid curves represent a calculation based upon the dispersion relation given by Eq. (10). The solid points represent data in the orientation of branch 2. The solid line for branch 1 was obtained from the fit to branch 2 as described in Sec. III B 3. The [100], [111], and [110] directions apply to branch 1 only. The low-frequency points are second-band data.

sents the [111] frequency (the minimum in extremal cross section), and $C_2 = C$. If $C_2 = 0$ the surface is cylindrically shaped.

$C_1$ and $C_2$ are determined by a least-squares fit of Eq. (11) to the data. Since the [111] direction was known to only $\pm 3°$ as a function of sample rotator angle, a more exact minimum in frequency was determined in the following two different ways.

(i) Crystal symmetry requires that the frequencies of the pockets at [111] and [11$\bar{1}$] be the same when the field is along [110]. Since branches of both pockets were generally observed around [110], the crossing of the branches could be used to determine the [110] direction. The [001] direction could be obtained in the same manner. If only well-defined crossings were considered, then the scatter among the angles at which the crossings of the various branches ($B$, $C$, $D$, $E$) occurred was $\pm \frac{1}{2}°$. The two orientations of sample 1001A determined from the [110] and the [001] crossing differed by less than a degree.

(ii) Samples for which this crossing was not observed (sample 670 and those for $p^* \geq 6.1 \times 10^{20}$ cm$^{-3}$) had the [111] direction determined by select-

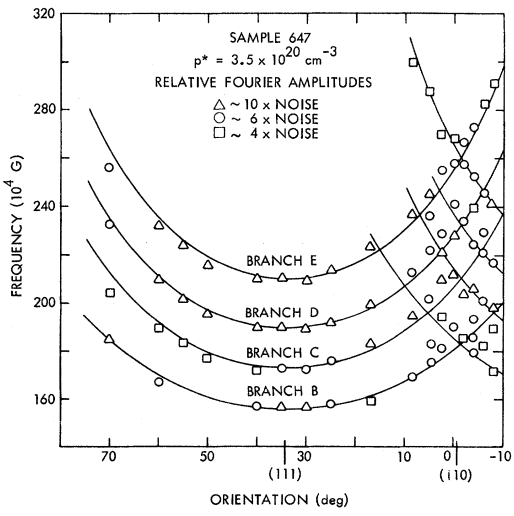


FIG. 7. dHvA frequencies vs orientation. The solid curves represent a calculation based upon the dispersion relation given by Eq. (10).

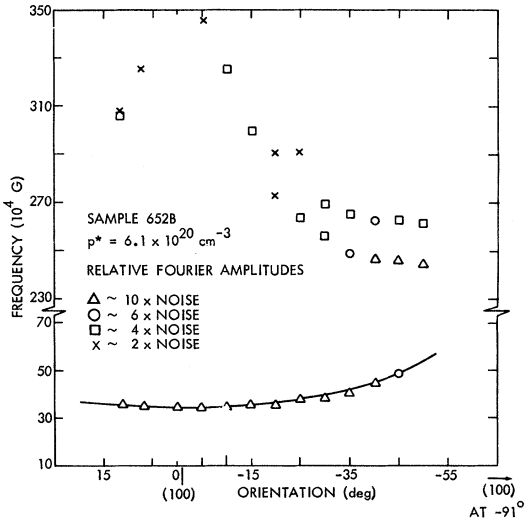


FIG. 9. dHvA frequencies vs orientation. Solid curve represents a calculation based upon the dispersion relation given by Eq. (10). The low branch is second-band data.

TABLE II. Parametric representation of the data. $C1$, $C_2$, and $\theta_0$ are the parameters of Eq. (11). The quadratic mean error (QME) is the rms value of the deviation of Eq. (11) from the data points. The axis of rotation is $[1\bar{1}0]$ except when noted.

| Branch | Sample | Field range ($10^4$ G) | Angular range, $\theta$ (deg) | $\theta_0$ (deg) | $C_1$ ($10^4$ G) | $C_2$ | QME ($10^4$ G) | [111] SdH frequency ($10^4$ G) |
|---|---|---|---|---|---|---|---|---|
| $B$ | 1001A | 3–8 | 88 to 10 | 35.0 | 74.9 | 0.19 | 1.4 | |
| $C$ | 1001A | 3–8 | not observed in dHvA | | | | | |
| $D$ | 1001A | 3–8 | 88 to −4 | 35.0 | 117.6 | 0.04 | 0.8 | |
| $E$ | 1001A | 3–8 | 88 to −4 | 35.0 | 144.8 | 0.05 | 1.7 | |
| $B$ | 1000 | 1.2–2.5 | 45 to −4 | 33.6 | 82.2 | −0.09 | 0.6 | |
| $C$ | 1000 | 1.2–2.5 | 55 to −4 | 33.6 | 109.6 | 0.14 | 0.5 | |
| $D$ | 1000 | 1.2–2.5 | 55 to −4 | 33.6 | 124.6 | 0.10 | 0.5 | |
| $E$ [a] | 1000 | 1.2–2.5 | 55 to −4 | 33.6 | 151.2 | 0.08 | 1.2 | |
| $B$ | 676 | 1–2 | 93 to −8 | 33.5 | 84.8 | 0.03 | 1.5 | 89 |
| $C$ | 676 | not observed in dHvA at low fields | | | | | | |
| $D$ [a] | 676 | 1–2 | 93 to −8 | 33.5 | 128.1 | 0.01 | 1.0 | 133 |
| $E$ [a] | 676 | 1–2 | 95 to −8 | 33.5 | 154.9 | 0.01 | 0.8 | 160 |
| $B$ [a] | 676 | 4–10 | too much scatter for a good representation | | | | | 89 |
| $C$ | 676 | 4–10 | observed only at [110] in dHvA | | | | | 110 |
| $D$ [a] | 676 | 4–10 | 76 to −8 | 34.5 | 130.1 | 0.02 | 1.3 | 133 |
| $E$ [a] | 676 | 4–10 | 76 to −8 | 34.5 | 158.4 | 0.05 | 1.5 | 160 |
| $B$ | 670 | 1–1.5 | 75 to 0 | 34.9 | 97.5 | 0.11 | 1.9 | 99 |
| $C$ | 670 | 1–1.5 | observed only at [110] at high fields in dHvA | | | | | 119 |
| $D$ [a] | 670 | 1–1.5 | 75 to 0 | 34.9 | 140.5 | 0.04 | 2.1 | 140 |
| $E$ [a] | 670 | 1–1.5 | 75 to 0 | 34.9 | 167.1 | 0.00 | 1.4 | 167 |
| $B$ | 647 | 3–7.5 | 8 to 70 | 34.5 | 155.6 | 0.17 | 1.6 | |
| $C$ | 647 | 3–7.5 | 8 to 70 | 34.5 | 172.8 | 0.02 | 1.8 | |
| $D$ [a] | 647 | 3–7.5 | 8 to 70 | 34.5 | 189.6 | −0.01 | 0.9 | |
| $E$ | 647 | 3–7.5 | −8 to 70 | 34.5 | 210.3 | −0.05 | 1.9 | |
| 1 | 652A | 4–10 | 35 to −35 | 11.3 | 199.6 | −0.07 | 1.3 | |
| 2 | 652A [b] | 4–10 | 35 to −4 | −0.2 | 204.0 | −0.05 | 1.1 | |
| Upper [a] | 652B [c] | 4–10 | 0 to −50 | −46.2 | 261.4 | 0.05 | 2.5 | |
| Lower | 652B [c] | 4–10 | 0 to −50 | −46.2 | 246.4 | −0.08 | 5.0 | |
| Second [a] band | 652B [c] | 4–10 | 11 to −45 | −1.2 | 35.36 | −0.02 | 0.4 | |
| 1 [a] | 1002 | 5–10 | −36 to 25 | 11 | 221.3 | 0.02 | 1.5 | |

[a] Data can be as well fit with $C_2 = 0$.
[b] Rotated in the plane given in the text (Sec. III B 2).
[c] Rotated approximately about a ⟨100⟩ axis.

ing the $\theta_0$ in Eq. (11) for which the quadratic mean error was a minimum.

All of the data were fit using method (ii) to see if there was any systematic deviation of the minima of the different branches from each other. None was observed. The results of method (ii) had more scatter ($\pm 2^\circ$ in general) than method (i). Therefore, method (i) was used even though the sample rotator accuracy was involved. In any event, the two methods gave good agreement as to the angular position of the minimum.

With $p^* \geq 6.1 \times 10^{20}$ cm$^{-3}$ the data describing a single pocket had one branch instead of four. The axis of rotation was again $[1\bar{1}0]$ for sample 1002 and for branch 1 of sample 652A (here branches 1 and 2 result from two runs with different axes of rotation).

With $p^* \geq 6.1 \times 10^{20}$ cm$^{-3}$ oscillations of a smaller set of pockets appeared with a minimum frequency in a ⟨100⟩ direction. These are called "second-band" oscillations and are so labeled in Table II, though they are probably another set of pockets in the same band (Sec. I) as the "first-band" oscillations (the pockets seen at all carrier concentrations). The first-band oscillations in sample 652B show a splitting because the axis of rotation is not quite [100].

### 3. *Adequacy of Dispersion Relation*

Since data were taken on sample 652A for two different orientations, Eq. (10) can be checked for consistency using Eq. (11). Branch 2 has a plane of rotation normal to the plane of rotation of branch 1 and intersects it 11.5° from [111] toward [001]. The parameters of branch 2, $C_1$ and $C_2$, as determined from the least-squares fit to Eq. (11), are related by Eqs. (12) and (13) to the parameters $C_1'$ and $C_2'$ that should be observed at the orienta-

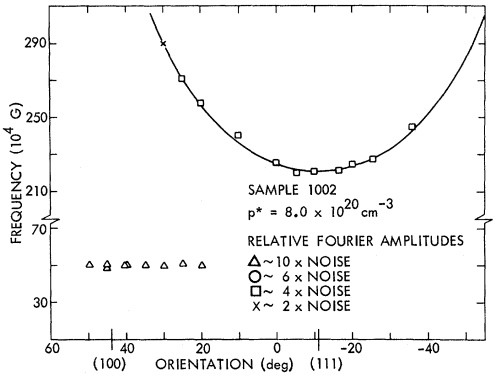


FIG. 10. dHvA frequencies vs orientation. Solid curve represents a calculation based upon the dispersion relation given by Eq. (10). The low branch is second-band data.

tion of branch 1 by

$$C_2' = C_2 \cos^2(\gamma)/(1 - C_2 \sin^2\gamma)$$

and

$$C_1' = (C_2'/C_2)^{1/2}\, C_1 .$$

For $\gamma = 11.5°$ one obtains for $C_1'$ and $C_2'$, $199.7\times10^4$ G and $-0.045$ as compared to the measured values $199.6\times10^4$ G and $-0.07$ given in Table II. The $11.5°$ value for $\gamma$ was obtained by subtracting the rotator angle at which the minimum frequency of branch 1 occurred from the angle of the crossing of branch 1 with branch 2 (Fig. 8). Since this crossing was used as the angle of the minimum frequency $\theta_0$ of branch 2, and the crossing of the branches is somewhat affected by the choice of the minimum, the final value of $11.5°$ had to be arrived at self-consistently. The value of $11.5°$ for $\gamma$ is probably not determined to better than $\pm 1°$. Changes in $\theta_0$ of this size lead to an error of $\pm 0.4\%$ in $C_1$, while $C_2$ is unaffected.

### C. Effective Masses and Dingle Temperatures

With $p$ above $3\times10^{20}$ cm$^{-3}$, single-period data with no second harmonic were obtained. Around the [111] direction no second-band oscillations were present, while around [001] no first-band oscillations were observed (except at very high fields). The envelope showed no modulation. This set of circumstances presented an opportunity to measure masses and Dingle temperatures associated with the first and second bands.

Owing to an orientation error which occurred when sample 652A was cut from the original crystal, the first-band mass and Dingle temperature [Eqs. (8) and (9)] were measured $11.5°$ from [111] toward [001]. The second-band mass and Dingle temperature were measured at [001] in sample 652B. These parameters are listed in Table III. The associated frequency in Table III is the frequency measured in the same direction as the mass, as is the frequency of sample 1002. The frequency of sample 1002 is used to determine the change in frequency with carrier concentration for bands 1 and 2.

In making the calculations below we assume that samples 652A and 652B are identical. They were cut from the same wafer, plated with as nearly the same amount of Sn as possible, and annealed in the same quartz ampoule. The second-band frequencies are very close at [001]. If the mass $m$ does not change too rapidly with energy and the rigid-band approximation holds, then

$$m \approx (\hbar^2/2\pi)\, \Delta A/\Delta E \tag{14}$$

and

$$m_1/m_2 \approx \Delta F_1/\Delta F_2 . \tag{15}$$

Here, for a change in carrier concentration, $\Delta p = 0.6\,\Delta p^*$, $\Delta A$ is the change in cross-sectional area, $\Delta E$ is the change in Fermi energy, $\Delta F$ is the change in frequency, and subscripts 1 and 2 refer to the first and second bands, respectively. From Table III, $m_1/m_2 = 0.75$, and $\Delta F_1/\Delta F_2 = 0.66$. The two ratios differ by 13% which is within experimental error. If we calculate a ⟨111⟩ first-band frequency for sample 652B from the dHvA data and again compare the above two ratios, the agreement is no worse.

A density of states at the FS $\Delta p/\Delta E$ can be calculated from Eq. (14):

$$\Delta p/\Delta E = (\mathrm{cm}/e\hbar)\,(\Delta p/\Delta F) = 6\times10^{21}\ \mathrm{eV^{-1}\,cm^{-3}}. \tag{16}$$

## IV. DISCUSSION

The data divide into two groups, the high-carrier-concentration data from samples with $p$ above $3\times10^{20}$ cm$^{-3}$ and the low-carrier-concentration data below $3\times10^{20}$ cm$^{-3}$. The high-carrier-concentration data include the cyclotron masses, Dingle temperatures, density of states, and single-period data (one pocket giving rise to one branch of frequencies). The low-carrier-concen-

TABLE III. The masses, Dingle temperatures, and frequencies of the first and second bands for $p^* = 6.1 \times 10^{20}$ cm$^{-3}$ and the frequencies for $p^* = 8.0\times10^{20}$ cm$^{-3}$.

| Band | $m/m_0$ | Dingle temperature (K) | Associated frequency ($10^4$ G) | Frequency of sample 1002 ($10^4$ G) | $\Delta F$[a] ($10^4$ G) |
|---|---|---|---|---|---|
| 1 | $0.125 \pm 0.012$[b] | $21.6 \pm 2.1$[b] | 204[b] | 226 | 22 |
| 2 | $0.094 \pm 0.009$[c] | $17.3 \pm 1.7$[c] | 35.4[c] | 50.0 | 14.6 |

[a]The change in frequency with carrier concentration for the orientations given in the text.

[b]Data from sample 652A.

[c]Data from sample 652B.

tration data include the multiperiod data (one pocket at $L$ giving rise to several branches) with its possibly anomalous harmonic content.

### A. High-Carrier-Concentration Single-Period Data

#### *1. Second Band*

A study of the transport properties of SnTe [22] indicates that the Fermi level enters a second valence band at $p^* = 2.2\times10^{20}$ cm$^{-3}$ (this value of $p^*$ will be called $p_C^*$). We observed second-band oscillations at the two highest carrier concentrations (samples 652A, 652B, and 1002). These oscillations describe a pocket elongated in a ⟨100⟩ direction. If the second band is assumed parabolic, the Fermi level at a carrier concentration of $3.6\times10^{20}$ cm$^{-3}$ measured relative to the energy at which the second band becomes populated is

$$\Delta E_F = \hbar F/mc = 0.043 \text{ eV}.$$

The values for $F$ and $m$ are from Table III. If our value of the density of states is used with $\Delta E_F$ a value of $1.8\times10^{20}$ cm$^{-3}$ is obtained for $p_C^*$.

The band calculations previously cited show secondary valence-band maxima on $\Sigma$ and tertiary maxima on $\Delta$. The amplitude of the second-band oscillations is quite large when the field is in a ⟨100⟩ direction. The calculated signal [19] for the first band agreed to within a factor of 2 with the data, when our values for the mass, Dingle temperature, $C$, and frequency were used. Even if we assume four symmetry-related pockets are contributing to the signal (as there would be for pockets on $\Sigma$), the signal is still large enough to be consistent with the fairly anisotropic pockets the frequency data describe.

When sample 652B is rotated about an axis approximately parallel to the [100] direction (Fig. 9), the second-band data of sample 652B remain single period, i.e., no beating was observed over about eight oscillations in the data. The sample is known to be misoriented 2° or 3° because of beating in the first-band data. The line shape in the transform is sharp and symmetrical from [001] to 5° past [011]. The line shape at approximately [011] is shown in Fig. 11. This absence of any beating favors a $\Delta$ point of the Brillouin zone as the location of the second-band pockets. However, it may be that there were not enough oscillations in the data to observe beating.

#### *2. Lifetime Considerations*

Oscillations in general were observed at lower fields than mobility considerations had lead us to anticipate. In sample 652A, for example, the helium conductivity mobility predicts $\omega_c\tau \approx 1$ at about 140 kG. Oscillations were observed at 40 kG. The helium conductivity mobility and the ratio $e\tau/m$ (evaluated from our measured values of the mass and Dingle temperature) have nearly the same value in sample 652A, even though two different quantities, the lifetime for impurity scattering and the relaxation time, are involved. Since this means that $\omega_c\tau \approx \frac{1}{3}$ at the onset of oscillations one might speculate that our measured value of the Dingle temperature is rather high. However, Braun *et al.* [23] have seen the same thing in tellurium (i.e., $\omega_c\tau \approx \frac{1}{2}$ at the onset of oscillations), and the calculated absolute amplitude of the first-band oscillations does check satisfactorily with experiment. It should be pointed out that carrier-concentration variations, strains, etc., increase the apparent value of the Dingle temperature.

#### *3. Density of States*

In Sec. III, the density of states at $p = 3.6\times10^{20}$ cm$^{-3}$ was calculated to be $6\times10^{21}$ (eV cm$^3$)$^{-1}$. Finegold *et al.* [24] have measured the heat capacity of SnTe from 0.2 to 0.5 K. They obtain a density of states of $9.2\times10^{21}$ (eV cm$^3$)$^{-1}$ at a carrier concentration of $7.8\times10^{20}$ cm$^{-3}$. If our value is altered according to the parabolic approximation to account for the difference in carrier concentration, we obtain $7.7\times10^{21}$ (eV cm$^3$)$^{-1}$. The valence band in SnTe is nonparabolic, but it is possible to show the correction for nonparabolicity is in the right direction. The density of states in the rigid-band approximation can be expressed as

$$D(E) = \frac{dp}{dE} \propto m\frac{dp}{dA}.$$

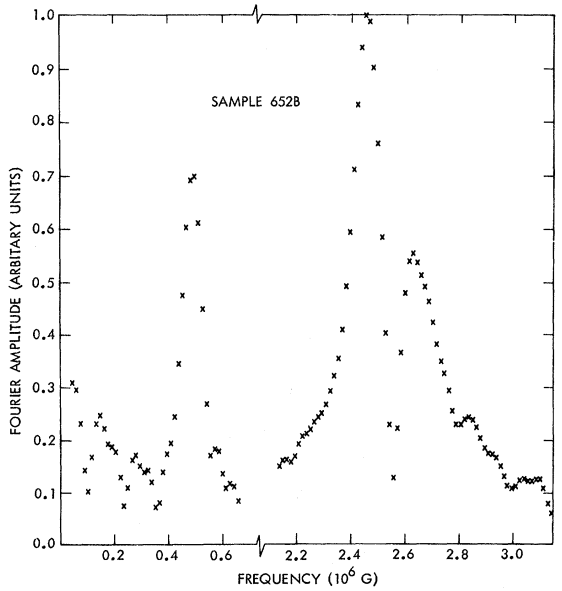


FIG. 11. Second-band line shape at approximately [011]. The first band shows a splitting due to a slight misorientation.

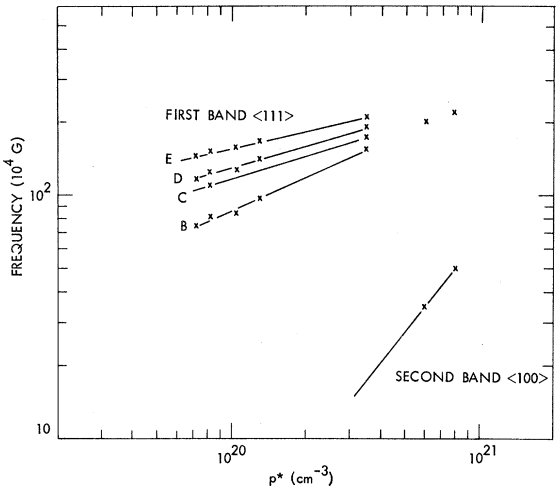


FIG. 12. First- and second-band minimum frequencies as a function $p^* = (Re)^{-1}$. $R$ is the low-field Hall coefficient measured at 77 K or lower.

If the ⟨111⟩ first-band frequencies of samples 625A and 1002 are used with the assumption of a power law for the dependence of the frequencies on carrier concentration, then $A \propto p^{0.3}$ (Fig. 12). If a constant cyclotron mass is assumed, our value for the density of states at a carrier concentration of $7.8\times10^{20}$ $cm^{-3}$ would be $12\times10^{21}$ $(eV\ cm^3)^{-1}$.

A density-of-states effective mass defined as

$$m_D = (\tfrac{1}{3}\pi)^{1/3}\ \pi\hbar^2 D(E_F) p^{-1/3}$$

has the value of $2m_0$ for our value of the density of states. This is the same as the value found at much higher carrier concentrations.[25] The high density-of-states effective mass is consistent with the ⟨111⟩ cyclotron mass and the almost cylindrical shape of the FS determined from the dHvA data.

From the above considerations we estimate the error in our value of the density of states to be ±25%. The first-band mass, carrier concentration, and frequencies were all involved in the calculation of the density of states. The agreement between the analysis of our data and the heat-capacity results corroborates our values for the masses and carrier concentrations.

### B. Low-Carrier-Concentration Multiperiod Data

#### *1. Characteristics of Data*

For $p < 3\times10^{20}$ $cm^{-3}$ a number of frequencies describing one pocket at $L$ were observed. The frequencies of the different branches ($B$, $C$, $D$, $E$) have several anomalous features. The branches are roughly parallel to each other in the sense that no coalescence (or incipient coalescence) is observed. The branches have a cutoff occurring at approximately ±55° from ⟨111⟩, which is independent of carrier concentration. Branches $B$, $D$, and $E$ have comparable amplitudes while $C$ is weak. Branch $C$ was seen at the orientations at which the other branches were seen only in samples 1000 and 647. The frequencies, when observed in dHvA, are the same as in SdH. There is a small discrepancy around ⟨110⟩ in sample 676 (Fig. 5) between the SdH and the dHvA data which we attribute to a misorientation of the sample in the SdH experiment. In samples 670 and 676 branch $C$ was seen at all orientations in SdH but in dHvA was seen only in sample 670 around ⟨110⟩ at high fields. A large-amplitude additional branch, branch $A$, was seen in SdH in sample 670 only. In dHvA branch $A$ was seen with a relatively weak amplitude and at only a few orientations.

Another sample, sample 677, was examined with SdH at 1.2 K.[26] Although the data are replete with unidentifiable points there appear to be frequencies from symmetry-related pockets not observed in any other work; i.e., with the field sweeping from [110] to [001]. Branches $D$ and $E$ were possibly observed from pockets at $[1\bar{1}1]$ and $[\bar{1}\bar{1}1]$ over part of the sweep.

An interesting observation is shown in Table IV. The ⟨111⟩ frequencies are listed for each branch at five carrier concentrations. The various differences in the ⟨111⟩ frequencies are listed also. The ⟨111⟩ frequencies at the four lowest carrier concentrations increase with increasing carrier concentration, while the differences at each carrier concentration remain constant. Furthermore, within experimental error, all the differences are integral multiples of 140 kG. It should be pointed out that these four samples were prepared separately. Sample 676 had the excess Sn removed after annealing by method (ii) of Sec. II. It was then annealed again. This procedure was not used on the other samples. The principal difference in the preparation of samples 676 and 1000 was the additional vacuum anneal of sample 676. The dHvA data indicate that the difference in carrier concentration between the two samples is not as great as that indicated in Table I. The SdH branch-$C$ ⟨111⟩ values do not fit this pattern. The pattern is maintained in branches $B$, $D$, and $E$ of the SdH data (including sample 677). Branch $A$ of sample 670 is 140 kG below branch $B$.

Sample 647 deviates markedly from the pattern. However its carrier concentration is 2.5 times greater than the next lowest carrier concentration (sample 670). A consequence of this is that the second band has become populated and the lattice constant is 0.15% less than that in sample 670.[27] At this time we have no explanation for the multiperiod data. Some of the explanations which have been proposed will be discussed below.

TABLE IV. dHvA ⟨111⟩ frequencies and frequency differences in units of $10^4$ G. The letters $B$, $C$, $D$, and $E$ designate branches as described in the text. The lower line sets off sample 647 which has a carrier concentration 2.5 times greater than that of sample 670.

| Sample | $E$ | $D$ | $C$ | $B$ | $E-D$ | $E-C$ | $E-B$ | $D-C$ | $D-B$ | $C-B$ |
|---|---|---|---|---|---|---|---|---|---|---|
| 1001A | 145 | 118 | ··· | 75 | 27 | ··· | 70 | ··· | 43 | ··· |
| 1000 | 151 | 125 | 110 | 82 | 27 | 42 | 69 | 15 | 43 | 28 |
| 676 | 155 | 128 | ··· | 85 | 27 | ··· | 70 | ··· | 43 | ··· |
| 670 | 167 | 141 | ··· | 97 | 26 | ··· | 70 | ··· | 44 | ··· |
| 647 | 210 | 190 | 173 | 156 | 20 | 37 | 54 | 17 | 34 | 17 |

### 2. *Possible Explanations for Multiperiod Data*

Muldawer[28] has found a low-temperature phase transition from a cubic to a rhombohedral structure at low carrier concentrations. A powder with $p^* = 8\times10^{20}$ cm$^{-3}$ did not transform but a powder with $p^* = 1\times10^{20}$ cm$^{-3}$ did. This is consistent with the neutron diffraction work[29] in which the temperature softening of a transverse optical phonon mode was observed with $p^* = 8\times10^{20}$ cm$^{-3}$. The phase transition found by Muldawer is a possible explanation of the multiperiod data. This explanation was previously proposed by Stiles and Esaki.[30] Figure 12 shows the transition from multiperiod to single-period data. Multiperiod data due to sample inhomogeneity have been observed in alloys of PbTe and SnTe.[31] However, the amplitudes in the samples yielding multiperiod data are an order of magnitude smaller than those yielding single-period data, even though the mobilities are not much different.[32]

In Sec. IV A 2, it was shown that the $(\tau/m)_{\text{transport}}$ computed from transport measurements had nearly the same value as $\tau/m$ in the first band at a carrier concentration of $p = 3.6\times10^{20}$ cm$^{-3}$. The field at the onset of oscillations was significantly lower than or equal to that predicted by $(eH/c)(\tau/m)_{\text{transport}} = 1$ in samples 1000, 676, 670, and 647. In sample 670 oscillations were observed at 9 kG, while the above relation is satisfied at 14 kG. Small-angle scattering affects dHvA amplitudes more than it affects the magnitude of the resistivity of the sample. Since dHvA is a bulk effect the samples must be locally homogeneous to have oscillations at such low fields. If the explanation of the extra frequencies is sample inhomogeneity, the inhomogeneity must be a reproducible domainlike structure. It is difficult to see how inhomogeneities due to a phase change or poor material preparation can lead to the ordered array of numbers presented in Table IV.

### 3. *Harmonic Content*

The characteristic feature of the harmonic content is its low amplitude. A calculation shows that if the spin-splitting factor $\cos(\pi mg/2m_0)$ is set equal to unity, second and third harmonics [$l = 2$ and 3 in Eq. (3)] should be observed at high fields in the low carrier-concentration samples. In sample 676 oscillations were observed below 10 kG. The second harmonic was either missing or no more than 20% of the main peaks in field sweeps to 100 kG. The third harmonic was not observed. Whenever the second harmonic was observed it was accompanied by frequencies that were the sum of frequencies from two different branches. These sum frequencies have about the same amplitude as the second harmonic. In sample 677 many sum and difference frequencies are present. The harmonics are almost completely absent. It is not clear therefore what the origin of the second harmonic is in these data.

If the harmonic content is not anomalously low, then the following conditions on $mg$ minimize the second and third harmonic amplitude relative to the first:

$$\frac{\cos 2g^*}{\cos g^*} \approx \frac{\cos 3g^*}{\cos g^*} \approx 0.4 ,$$

where $g^*$ is $\pi mg/2m_0$. From this we can estimate that $g^*/\pi - \text{integer} \approx \pm 0.2$ in samples 1001A and 676. The term $g^*$ would have to be approximately independent of orientation.

## C. Shape of First-Band Surface

The surface generated from the Rabii dispersion relation[6] was similar to the surface described by the data. Since that time corrections to this dispersion relation have negated that agreement.[33]

The surface posed by Tsu, Howard, and Esaki[7] (THE) shows rough agreement with the frequency and cyclotron mass data when comparison is made with Fig. 12 of that reference. The surface of THE changes from a "dumbbell" at high carrier concentrations to a convex surface at low carrier concentrations. This corresponds to $C$ changing from minus to plus. An examination of Table III shows this trend. In fact, if one examines $C$ as a function of $C_1$ (the ⟨111⟩ frequency) this trend is more pronounced. This shape evolution leads to

an additional ⟨111⟩ frequency as the carrier concentration increases. No additional ⟨111⟩ frequency was observed. Poor $\omega_c\tau$ conditions could reduce the amplitude of these cross sections too much to be seen. However, THE assume the second band is at $L$. This is unlikely in view of the ⟨100⟩ orientation of these surfaces. There are other objections to this model.[34]

Because of its nature, the Tung and Cohen[9] calculation can be compared with the data at a carrier concentration of $1\times10^{20}$ cm$^{-3}$ only (sample 670). The ⟨111⟩ frequency of the calculated surface is nearly a factor of 2 larger than the highest ⟨111⟩ frequency of sample 670. The surface is oblate instead of prolate, i.e., the frequencies would deviate considerably from those observed with the field rotated further than ±30° from ⟨111⟩ even if the ⟨111⟩ frequency were correct.

In the Dimmock calculation[8] the ⟨111⟩ frequencies have about a $p^{0.75}$ dependence on carrier concentration. The 0.75 exponent is roughly double that of the data. The evolution of the shape of the Dimmock surface described previously does not correspond to that described by the data. However, the carrier concentrations considered here are rather high for a $\vec{k}\cdot\vec{p}$ calculation.

## V. SUMMARY

We have been able to make oscillatory FS measurements over a wide range of carrier concentrations ($5\times10^{19}$–$5\times10^{20}$ cm$^{-3}$). The mobilities of some of the samples were lower than that thought necessary to obtain useful data with the range of magnetic fields available. For the first time quantitative information was obtained on the shape of the surface, ⟨100⟩ cyclotron mass, and ⟨100⟩ lifetime in the second band. Much additional information was obtained on the shape of the first-band surface, and the ⟨111⟩ cyclotron mass and a lower bound on the scattering lifetime were measured for the first time. If a carrier-concentration-dependent phase change is responsible for the anomalous first-band data, then we have established that the carrier concentration above which SnTe does not transform from the NaCl structure lies between $2.1\times10^{20}$ and $3.6\times10^{20}$ cm$^{-3}$.

## ACKNOWLEDGMENTS

The authors thank Dr. Julius Babiskin and P. G. Siebenmann for helping make the SdH measurements at the Naval Research Laboratory. We also thank Dr. J. R. Dixon and Dr. R. S. Allgaier for many helpful discussions. We thank R. Greer and the Goddard Space-Flight Center for digitizing the data, W. Fiske for machining the sample holder, E. Davis for winding the necessary coils, and Mrs. E. Reidinger for typing the manuscript.

---

†Work constitutes part of a thesis submitted to the University of Maryland, College Park, Maryland, by H. T. Savage in partial fulfillment of the requirements of the Ph.D. degree in Physics.

*Work supported by the Naval Ordnance Laboratory Independent Research Funds.

[1]Naval Ordnance Laboratory Technical Report No. 64-30, p. 25 (unpublished); available from the Naval Ordnance Laboratory, Library Documents Division, Silver Spring, Md. 20910.

[2]N. J. Parada and G. W. Pratt, Phys. Rev. Letters 22, 180 (1969).

[3]B. B. Houston, Jr., R. S. Allgaier, J. Babiskin, and P. G. Siebenmann, Bull. Am. Phys. Soc. 9, 60 (1964).

[4]R. F. Brebrick, J. Phys. Chem. Solids 32, 551 (1971).

[5]Y. W. Tung and Marvin L. Cohen, Phys. Rev. 180, 823 (1969).

[6]Sohrab Rabii, Phys. Rev. 182, 821 (1969).

[7]R. Tsu, W. E. Howard, and L. Esaki, Phys. Rev. 172, 779 (1968).

[8]J. O. Dimmock, in *The Physics of Semimetals and Narrow-Gap Semiconductors*, edited by D. L. Carter and R. T. Bate (Pergamon, New York, 1971), p. 319.

[9]Y. W. Tsang and M. L. Cohen, in Ref. 8, p. 303.

[10]F. Herman, R. L. Kortum, I. B. Ortenburger, and J. P. Van Dyke, J. Phys. (Paris), Colloq. 29, C4-62 (1968).

[11]R. L. Bernick and L. Kleinman, Solid State Commun. 8, 569 (1970).

[12]M. L. Cohen, Y. Tung, and P. B. Allen, J. Phys. (Paris) Suppl. 29, C4-163 (1968).

[13]W. Paul, J. Phys. (Paris), Colloq. 29, C4-171 (1968).

[14]L. M. Roth and P. N. Argyres, in *Semiconductors and Semimetals*, edited by R. K. Willardson and A. C. Beer (Academic, New York, 1966), p. 159.

[15]J. R. Burke, B. B. Houston, H. T. Savage, J. Babiskin, and P. G. Siebenmann, J. Phys. Soc. Japan 21, 384 (1966).

[16]J. R. Burke, B. Houston, H. T. Savage, J. Babiskin, and P. G. Siebenmann, Bull. Am. Phys. Soc. 14, 329 (1969).

[17]A. D. Brailsford, Phys. Rev. 149, 456 (1966).

[18]I. M. Lifshitz and A. M. Kosevich, Zh. Eksperim. i Teor. Fiz. 29, 730 (1955) [Sov. Phys. JETP 2, 636 (1956)].

[19]A. Goldstein, S. J. Williamson, and S. Foner, Rev. Sci. Instr. 36, 1356 (1965).

[20]A. C. Thorsen and T. G. Berlincourt, Rev. Sci. Instr. 34, 435 (1963).

[21]Naval Ordnance Laboratory Technical Report No. 70-119 (unpublished); available from the Naval Ordnance Laboratory, Library Documents Division, Silver Spring, Md. 20910.

[22]R. S. Allgaier and B. Houston, Phys. Rev. B 5, 2186 (1972); A. Sagar and R. C. Miller, *Report of the International Conference on the Physics of Semiconductors, Exeter* (The Institute of Physics and Physical Society, London, 1962), p. 653.

[23]E. Braun, G. Landwehr, and L. J. Neuringer, in *Proceedings of the Conference on High Magnetic Fields and Their Applications* (The Institute of Physics and Physical Society, Nottingham, England, 1969), p. 77.

[24]L. Finegold, J. K. Hulm, R. Mazelsky, N. E. Phillips, and B. B. Triplett, Ann. Acad. Sci. Fennicae A 6, 129 (1966).
[25]J. K. Hulm, in NRL Report No. 6972, p. 30 (unpublished), available from the Naval Research Laboratory, Washington, D. C. 20390.
[26]J. R. Burke, B. Houston, and H. T. Savage, Bull. Am. Phys. Soc. 14, 329 (1969).
[27]R. F. Bis and J. R. Dixon, J. Appl. Phys. 40, 1918 (1969).
[28]L. Muldawer, Bull. Am. Phys. Soc. 16, 84 (1971).
[29]G. S. Pawley, W. Cochran, R. A. Cowley, and G. Dolling, Phys. Rev. Letters 17, 753 (1966).
[30]See comment at end of Ref. 14.
[31]J. R. Burke, J. D. Jensen, and B. B. Houston, in Ref. 8, p. 393.
[32]J. R. Burke and J. D. Jensen (private communication).
[33]S. Rabii (private communication).
[34]R. F. Bis and J. R. Dixon, Phys. Rev. B 2, 1004 (1970).

PHYSICAL REVIEW B VOLUME 6, NUMBER 6 15 SEPTEMBER 1972

# Excitonic Effects in Landau Transitions at the $E_1$ Edges of InSb and GaSb†

S. O. Sari*
*Joseph Henry Physics Laboratory, Princeton University, Princeton, New Jersey* 08540
(Received 12 November 1971)

Measurements are presented of differential reflectivity in a strong magnetic field in InSb and GaSb at the $E_1$ and $E_1+\Delta_1$ edges. A description of the circular-polarization modulation technique used to obtain the data is given. Optical absorption at a critical point along the [111] direction in a semiconductor lacking inversion symmetry is discussed. An exciton model in a magnetic field is developed. Numerical solutions for the first four bound-state energies having azimuthal quantum number $m=0$ are tabulated for the two-dimensional Schrödinger equation of an attractive Coulomb potential in a magnetic field. Solutions to the three-dimensional problem are discussed using the Born–Oppenheimer approximation. The exciton model is compared to experimental spectra of Landau levels at the $E_1$ edge of InSb. A value of $2.8\pm0.6$ meV is obtained for the exciton rydberg. This agrees with the value obtained using the measured effective transverse mass $m/\mu_t=19.7\pm1.3$ and the static dielectric constant of InSb. A lower limit on the longitudinal mass of $15\lesssim|\mu_l/\mu_t|$ is estimated. The sign of the longitudinal mass has not been unambiguously obtained; however, the critical-point symmetry at the $E_1$ edge may be of type $M_0$ instead of $M_1$. The $E_1$ excitonic energy gap is determined to be $2.015\pm0.001$ eV. Spectra of GaSb are compared to InSb. A line splitting of 33 meV due to the inversion asymmetry in GaSb is proposed.

## I. INTRODUCTION

Effects due to electromagnetic transitions between Landau levels were first observed in crystalline solids in cyclotron-resonance experiments in 1953[1] and in infrared magneto-optical experiments[2] a short time later. Extensive work has followed on optical magnetic effects,[3] yielding accurate measurements of band masses and a wealth of other band-structure parameters. Up to the present time quantized harmonic-oscillator levels have been seen only in the infrared. They have been studied at the lowest-energy-gap thresholds, and in transitions from the spin-orbit split-off valence bands[4,5] in a number of semiconductors. Attempts to look at higher bands have not resolved magnetic levels.[6]

In the present experiment, however, Landau levels are seen in the visible energy range at the $E_1$ edge in InSb.[7] The measurements have been obtained using an optical-polarization modulation technique, which is relatively noiseless. The method is not unlike other techniques used to make similar measurements,[8] but it has the virtue of requiring no modulation to be applied directly to the sample. In the present paper we have computed differential dielectric constants ($\Delta\epsilon_1$ and $\Delta\epsilon_2$) from our data. The "density of states" calculated from a model including excitons in a magnetic field has been compared to $\Delta\epsilon_2$. This approach has been necessitated by previous evidence for strong Coulomb effects at the $E_1$ thresholds.[9] A discussion of inversion asymmetry along the $\Lambda$ direction has been included in the analysis. This may be important in interpreting new observations of optical transitions in semiconductors lacking inversion symmetry.

The "edge" $E_1$ where Landau-level transitions are seen is shown in the energy-band-structure diagram of InSb in Fig. 1. It is away from the Brillouin-zone center in the [111] direction and has a valence-conduction gap of approximately 2 eV. The component split-off by the spin-orbit interaction is $E_1+\Delta_1$ about 0.5 eV higher. No Landau levels have been seen there thus far. The same statement may be made for still higher energy